Voltage and Current Limited Maximum Torque Algorithm of SPMSM in Traction Applications

Gabriel M. Pauka, Li Ding, Rui Liu and Yunwei (Ryan) Li
University of Alberta, Canada

***Abstract*-- permanent magnet synchronous machines (PMSMs) are widely used in traction applications on account of higher efficiencies, higher torque and power densities. Due to the reluctance torque component, internal PMSMs are commonly found; however, with the evolution of axial-flux PMSMs, machines with surface-mounted magnets are gaining relevancy. This paper developed a wide-speed operation algorithm for surface PMSMs that obtains the maximum mechanical torque possible while respecting the voltage and current constraints of the machine for any speed, named voltage and current limited maximum torque (VCLMT) algorithm, with an adjustable reference that produces a torque that ranges from zero to the maximum possible in all four torque-speed quadrants. The proposed VCLMT is verified and compared through both simulation and experiment.**

***Index Terms*-- voltage and current limited maximum torque (VCLMT), permanent magnet synchronous machine (PMSM), field-weakening operation.**

I. Introduction

Permanent magnet synchronous machines (PMSMs) are gaining popularity amongst electric vehicle (EV) manufacturers due to higher efficiencies, power and torque densities, and cooling capability [1]-[3]. To get a higher benefit from these figures of merit, interior permanent magnet synchronous machines (IPMSMs) are commonly utilized for traction applications due to their higher torque density and wider operation area than the surface permanent magnet synchronous machines (SPMSMs). However, with the evolution of axial-flux permanent magnet synchronous machines (AFPMSMs) for traction applications, SPMSMs became the machine that offers better figures of merit [4]-[5].

The wide speed control of a PMSM allows the machine to produce the maximum torque possible for all its operational speed ranges, respecting the machine's voltage and current limits. The PMSM has the ability to keep its torque at its maximum value from zero speed up to the base speed, where the back-electromotive force (back-EMF) induced by the permanent magnets reaches a magnitude in which the voltage-source converter (VSC) interfacing the DC and AC sides reaches its output limit. For speeds higher than the base speed, a field-weakening (FW) operation is needed, where it uses the machine currents not only to produce torque but also to weaken the permanent magnets. This results in a lower induced voltage that allows the machine to be controllable over the base speed, with the expense of a reduced torque. The need for a higher field-weakening – at the cost of a lower torque – increases with the machine speed.

An efficient strategy for controlling PMSMs is to control the machines in the rotor reference frame (RRF), also known as the dq-frame. For the operation below the base speed, the control is known as maximum torque per ampère (MTPA), where the reference currents for the control system do not depend on the machine speed. Normally the d-axis current reference is set to zero, and the q-axis current reference is related to the load.

For operation above the base speed, several FW controls are proposed. Some have the dq-frame current references created through a feedback technique, where a negative d-axis current is created using a closed-loop compensator that measures the stator voltage from the reference currents to the previous switching cycle and comparing it to the maximum value, increasing or decreasing the field-weakening [6]-[9]. Despite their simplicity, easy implementation, and precise steady-state operation, feedback FW control will has the disadvantage of needing some switching cycles to reach a steady-state point, allowing momentary controller saturation and less torque during transients.

To overcome the issues created by a feedback FW control, a more complex feedforward algorithm can be implemented, which consists in obtaining a new operating point within a switching cycle through calculations based on the machine parameters and behavior in the FW region [6]. One effective way to determine said behavior is to map the dq-frame currents in the dq-plane,[10]-[12]. This technique can be employed for both surface and interior PMSMs but is commonly found only for IPMSMs, named Voltage and Current Limited Maximum Torque (VCLMT), since there are simpler methods that provide satisfactory results for SPMSMs, such as the Constant-Voltage Constant-Power (CVCP) [13]-[14], which generates current references to keep the q-axis voltage constant using a simple equation that is a function only of the machine speed.

This paper develops a VCLMT algorithm for the SPMSM that allows a variable reference, which can generate any torque ranging from zero to the maximum possible for every speed while respecting the voltage and current constraints. It shows how the speeds at which the operation modes change is obtained, along with the maximum speed possible. Meanwhile, the impacts of a variable DC-link voltage in the torque and power profiles of the machine are discussed and compared to the proposed VCLMT algorithm with the commonly used CVCP in simulations and an experimental setup. The proposed

field-weakening method can maintain the stator voltage at its maximum value throughout the entire field-weakening region; thus, better utilizing the DC-link voltage and weakening the machine fluxes by only the necessary amount, without violating the current constraint and sacrificing less torque possible. Therefore, being able to generate more torque than the conventional method, and, consequently, more power as well.

II. Conventional CVCP Field Weakening

To illustrate the basic principle of FW methods, this section mainly investigated the conventional CVCP FW method, where the PMSM model and voltage and current trajectory are introduced. Then, following the trajectories, the d-q frame current references changed with speed is defined. To determine the preferred d-q axis, the current reference is key for the existing field weakening control method. The PMSM model in the d-q frame can be expressed as

$$\begin{cases} v_d = R_s i_d + \dfrac{d\lambda_d}{dt} - \omega_e \lambda_q \\ v_q = R_s i_q - \dfrac{d\lambda_q}{dt} + \omega_e \lambda_d \end{cases}; \quad \begin{cases} \lambda_d = L_d i_d + \lambda_{pm} \\ \lambda_q = L_q i_q \end{cases} \tag{1}$$

$$T_m = \frac{3}{2} p\left[(L_d - L_q) i_d i_q + \lambda_{pm} i_q \right] \tag{2}$$

where L_{dq} is the machine inductances in the dq-frame, i_{dq} is the machine currents in the dq-frame, λ_{dq} is the magnetic flux linkage in the dq-frame, λ_{pm} is the magnetic flux linkage created by the permanent magnets, R_s is the stator resistance, v_{dq} is the machine voltages in the dq-frame, ω_e is the machine electrical angular speed, T_m is the machine mechanical torque and p is the number of pole pairs.

A. Below the Base Speed: Maximum Torque per Ampère

For operation below the base speed $\omega_{e,base}$, the machine can achieve its maximum torque by decomposing $i_{s,ref}$ entirely in the q-axis. Therefore, the algorithm for the constant torque region can be denoted as

$$\text{MTPA Trajectory:} \begin{cases} i_{d,ref} = 0 \\ i_{q,ref} = i_{s,ref} \end{cases} \tag{3}$$

To allow a four torque-speed quadrant operation, $i_{s,ref}$ can either be positive (forward torque) or negative (backward torque), with $0 \le i_{s,ref} \le i_{s,max}$, where its magnitude indicating the amount of torque and signal indicates the direction of the torque created.

B. Above the Base Speed: Field-Weakening Mode

In steady-state and neglecting the resistive voltage drop, which the contribution will be considered in a future moment, the stator voltage v_s is given by $v_s = \sqrt{v_d^2 + v_q^2}$. According to (1), the stator voltage can be represented as

$$v_s = \sqrt{(\omega_e L_q i_q)^2 + (\omega_e L_d i_d + \omega_e \lambda_{pm})^2} \tag{4}$$

Equation (4) is solved for ω_e as

$$\omega_e = \frac{v_s}{\sqrt{(L_q i_q)^2 + (L_d i_d + \lambda_{pm})^2}} \tag{5}$$

Hence, it is defined as the base speed $\omega_{e,base}$, that dictates the maximum machine speed that can be obtained with the maximum output voltage of the VSC $V_{s,max}$ with the maximum stator current decomposed in the dq-frame by the MTPA algorithm, and it is given by

$$\omega_{e,base} = \frac{v_{s,\max}}{\sqrt{(L_q i_{s,\max})^2 + \lambda_{pm}^2}} \tag{6}$$

where $v_{s,\max} = (1 - s_m)\dfrac{V_{dc}}{\sqrt{3}} - R_s i_{s,\max}$, $i_{s,max}$ is the machine's maximum stator current, V_{DC} is the DC link voltage, and s_m is the safety margin. While for the MTPA algorithm the only constraint is the current, the voltage is also limited above the base speed. The commonly used CVCP conventional field-weakening algorithm for SPMSMs consists of injecting a negative d-axis current proportional to the machine speed, when above the base speed. The goal is to keep v_q constant at the FW region, resulting in $v_s \approx v_{s,max}$, since the d-axis voltage is small compared to the q-axis voltage.

$$\text{CVCP FW:} \begin{cases} i_{d,ref} = \dfrac{(\omega_{e,base} - |\omega_e|)\lambda_{pm}}{|\omega_e| L_d} \\ i_{q,ref} = \text{sgn}(i_{s,ref})\sqrt{i_{s,ref}^2 - i_{d,ref}^2} \end{cases} \tag{7}$$

It is possible to calculate the dq-frame currents and voltages created by this algorithm, which can be seen in Fig. 1 and 2, respectively. It can be seen in Fig. 2 that the q-axis voltage is constant, and v_s is close, but not equal, to $v_{s,max}$ in the FW region. Since it fails to utilize the maximum stator voltage, the speed range of the conventional CVCP method will be limited.

III. Proposed Wide Speed Operation of PMSMs

As can be seen, the q-axis voltage is constant, and v_s is close, but not equal, to $v_{s,max}$ in the FW region; this means

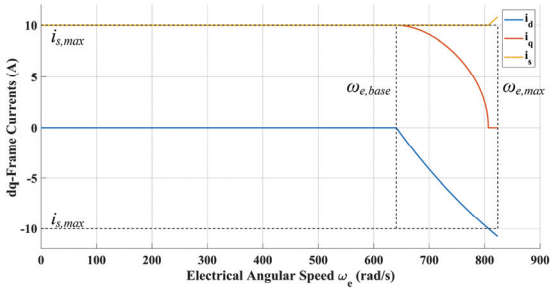

Fig. 1. CVCP dq-frame currents.

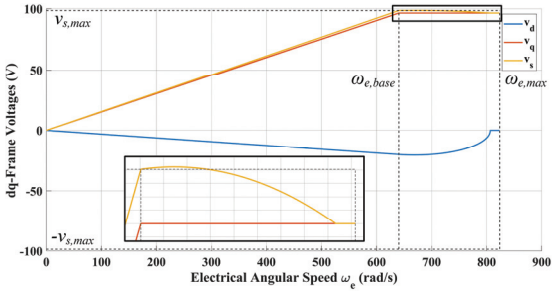

Fig. 2. CVCP dq-frame voltages, with zoom in the non-constant stator voltage after the base speed.

that the conventional CVCP field weakening method can not utilize the maximum stator voltage. Therefore, the operation range is limited. When the PMSM is operating at speeds above the base speed, the MTPA trajectory is not valid anymore, since it is not contained entirely inside of the VLC, as seen in Fig. 3.

By setting $v_s=v_{s,max}$ for better DC voltage utilization, from (5) it is possible to obtain

$$\left(\frac{i_d+I_{ch}}{v_{s,\max}/\omega_e L_d}\right)^2+\left(\frac{i_q}{v_{s,\max}/\omega_e L_q}\right)^2=1 \qquad (8)$$

where I_{ch} is the machine's characteristic current given by

$$I_{ch}=\frac{\lambda_{pm}}{L_d} \qquad (9)$$

Equation (9) defines an ellipse centered at ($-I_{ch}$,0) with horizontal radius $v_{s,max}/\omega_e L_d$ and vertical radius $v_{s,max}/\omega_e L_q$. Since $L_d=L_q$ for the SPMSM the ellipse becomes a circle, named *Voltage Limiting Circle* (VLC), as seen in Fig. 3. To respect the current and voltage constraints, the dq-frame current operating point must lie inside or at both the CLC and the VLC.

A. Partial Field-Weakening Operation

For illustration purposes, the system will have its parameters defined in Table I. The machine used is the Kollmorgen AKM 54K with reduced DC-link voltage (from its maximum of 640 Volts) and stator current (from its maximum of 13.72 A).

When the PMSM is operating at a speed above the base speed, the MTPA trajectory is not valid anymore, since it is not contained entirely inside of the VLC, as seen in Fig. 4.

However, for speeds above but close to $\omega_{e,base}$, part of the MTPA trajectory is still valid, also seen in Fig. 4. The MTPA trajectory lies partially inside of the VLC until the VLC crosses the origin. This speed is named *critical speed*, denoted by $\omega_{e,crit}$, and can be calculated as the VLC, in which the horizontal radius is equal in magnitude to the characteristic current. From (9) into the horizontal radius of (8),

$$\omega_{e,crit}=\frac{v_{s,\max}}{\lambda_{pm}} \qquad (10)$$

For any speed $\omega_{e,base}\le|\omega_e|\le\omega_{e,crit}$, the MTPA trajectory will still be partially valid, from $i_{s,ref}$ =0 to a current magnitude named as *cutoff current*, denoted as $i_{s,cut}$. The cutoff current can be calculated as the intersection point between the VLC of a speed $\omega_{e,base}\le|\omega_e|\le\omega_{e,crit}$ and the MTPA trajectory. By substituting (5) into (12) and solving for $i_d=i_{d,cut}$, the d-axis component of the cutoff current, can be obtained. Since the cutoff current lies in the MTPA trajectory, $i_{q,cut}$=0 and $i_{s,cut}=i_{d,cut}$. Thus

$$i_{s.cut}=\frac{v_{s,\max}}{|\omega_e|L_d}\sqrt{1-\left(\frac{\omega_e L_d}{v_{s,\max}}\right)^2} \qquad (11)$$

Therefore, for a speed $\omega_{e,base}\le|\omega_e|\le\omega_{e,crit}$ and a reference current $|i_{s,ref}|\le i_{s,cut}$, the trajectory followed is still the MTPA as seen in (5). However, for the same speed range of $i_{s,cut}\le|i_{s,ref}|\le i_{s,\max}$, the MTPA trajectory cannot be used, since that portion lies outside of the VLC and will violate the voltage limit constraint. For that current range, the trajectory must be the VLC itself. To obtain the equations to decompose the reference current $i_{s,ref}$ into an $i_{dq,ref}$ pair that lies over the VLC, it is substituted

$$i_{q,ref}=\sqrt{i_{s,ref}^2-i_{d,ref}^2} \qquad (12)$$

into (8), resulting in

$$\text{VLC Trajectory:}\begin{cases} i_{d,ref}=-\dfrac{i_{s,ref}^2}{2I_{ch}}+\dfrac{v_{s,\max}^2}{2\lambda_{pm}L_d\omega_e^2}-\dfrac{I_{ch}}{2} \\ i_{q,ref}=\operatorname{sgn}(i_{s,ref})\sqrt{i_{s,ref}^2-i_{d,ref}^2} \end{cases} \qquad (13)$$

The VLC trajectory created a non-zero $i_{d,ref}$ to weaken the machine's flux to respect the voltage constraint. By operating at the VLC, it can be guaranteed that the $i_{d,ref}$ has the smallest value possible, allowing more current at the q-axis to generate torque.

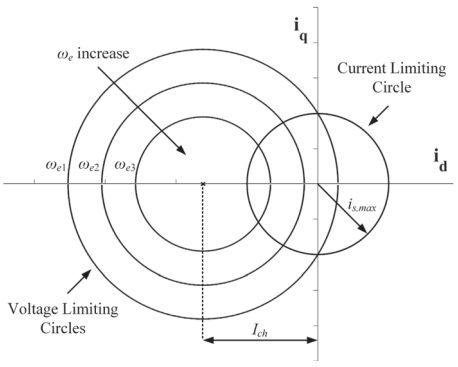

Fig. 3. CLC and VLCs for a SPMSM, with $\omega_{e1}<\omega_{e2}<\omega_{e3}$.

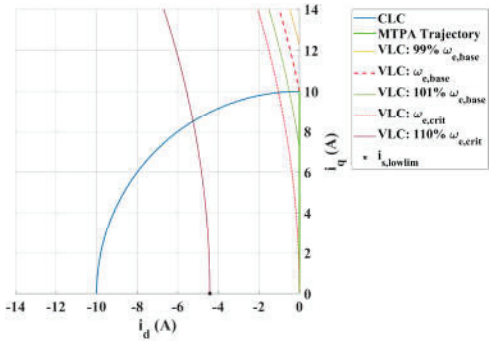

Fig. 4. VLC for a speed higher than the critical speed and $i_{s,lowlim}$.

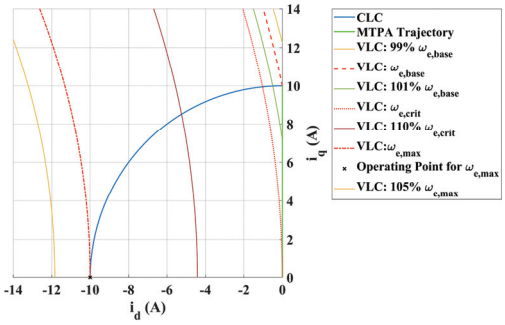

Fig. 5. VLC for the maximum speed and its only operating point

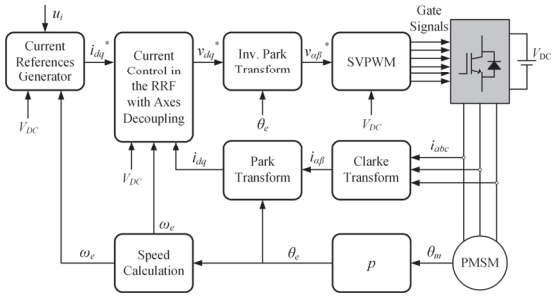

Fig. 6. Complete PMSM control system.

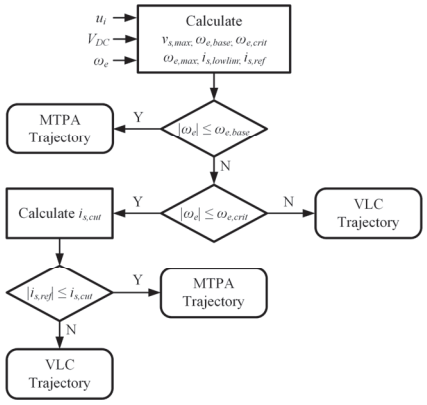

Fig. 7. VCLMT algorithm trajectory selector.

B. Full Field-Weakening Operation

For a speed $|\omega_e| > \omega_{e,crit}$,the MTPA trajectory lies completely out of the VLC; thus, cannot be used anymore. Also, for that speed range, the VLC does not have the origin at or inside it; therefore, the zero current vector is not possible – meaning that the minimal value for $i_{s,ref}$ cannot be zero anymore. The lower limit that the reference current can assume, which generates zero torque, is the intersection between the VLC and the d-axis, and it is given by the *lower limit current*

$$i_{s,low\lim} = I_{ch} - \frac{v_{s,\max}}{|\omega_e| L_d} \tag{14}$$

Thus, for $|\omega_e| > \omega_{e,crit}$, the only range of reference current possible is $i_{s,low\lim} \le |i_{s,ref}| \le i_{s,\max}$. The VLE and possible trajectory for this case can be seen in Fig. 5.

As the machine accelerates, the VLC shrinks to the point of completely leaving the CLC; this happens at the *maximum speed*, denoted as $\omega_{e,max}$ and is given by

$$\omega_{e,\max} = \frac{v_{s,\max}}{L_d (I_{ch} - i_{s,\max})} \tag{15}$$

The VLC for the maximum speed can be seen in Fig. 5, along with the only operation point possible for it. It is worth noticing in Fig. 5 that the only operating point possible for $|\omega_e| = \omega_{e,\max}$ lies over the d-axis; thus, no torque is produced. The PMSM which $I_{ch} > i_{s,\max}$, is characterized as a finite speed PMSM, since its torque reaches zero for a given speed. It is possible to see by (15) that the maximum speed becomes infinite for $I_{ch} = i_{s,\max}$,

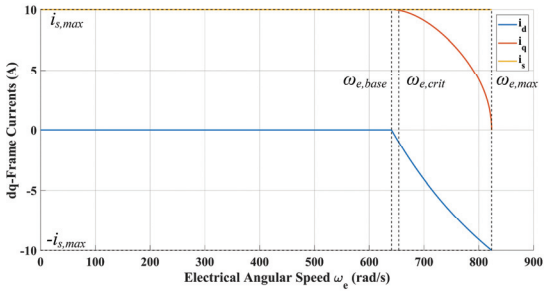

Fig. 8. VCLMT dq-frame currents.

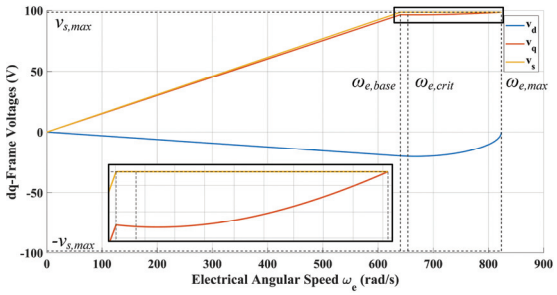

Fig. 9. VCLMT dq-frame voltages, with zoom in the constant stator voltage at its maximum value after the base speed.

and loses its meaning for $I_{ch} < i_{s,\max}$, since the VLC will always have some portion inside the CLC.

The complete control system is shown in Fig. 6, where u_i, V_{dc}, and ω_e are the inputs for current reference generation. To generate this reference, the *user input* u_i, ($-1 \le u_i \le 1$) is generated by the EV user. The detailed reference generation process and the decision tree for the algorithm is shown in Fig. 7.

By adopting the proposed VCLMT, the calculated dq-frame currents can be seen in Fig. 8, and the voltages in Fig. 9. Compared with Fig. 1 and Fig. 2, for the conventional CVCP method, that sets v_q=$v_{s,max}$, it shows that the total stator voltage violating its limit, and the q-axis current reaching zero before the maximum speed, meaning that the approximation made yielded an overvoltage and an under-torque operation in contrast with the proposed method. As a result, a wider speed operation can be achieved by the proposed method.

C. Comparison Between the Conventional and Proposed Methods

From (2) and knowing that the mechanical power P_m is given as $P_m = T_m\omega_m$, the torque and power profiles – the torque and power as a function of the machine speed – for each method are seen in Fig. 10 and 11, respectively.

It is possible to visualize that the proposed VCLMT algorithm presents a superior torque (and, by consequence, power) profile than the conventional CVCP in the field-weakening region, having more torque for the speeds in which the CVCP can operate and being able to reach a higher maximum speed as well. This is due to the fact that the VCLMT algorithm keeps the stator voltage constant at $v_{s,max}$ throughout the entire FW operation, as seen in Fig. 9, in contrast to the stator voltage that is below $v_{s,max}$ for most of the FW region from the CVCP, as seen in Fig. 2, meaning that the conventional algorithm weakened the

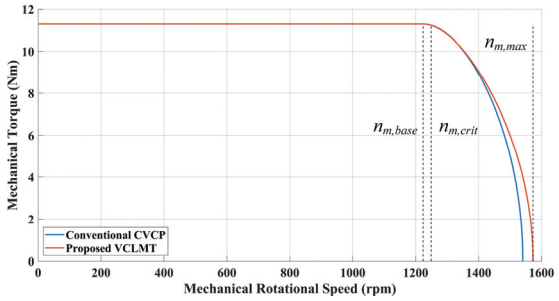

Fig. 10. Calculated torque profile comparison between algorithms.

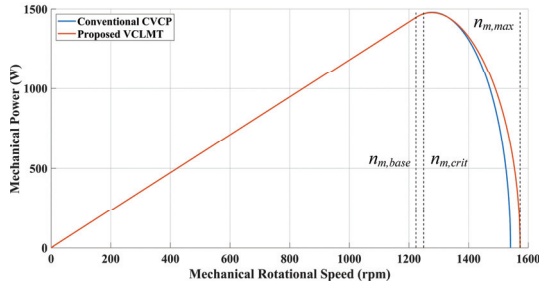

Fig. 11. Calculated power profile comparison between algorithms.

machine's magnetic flux more than needed, thus costing more torque.

IV. Experiment Results

Both algorithms are implemented in the system described in Table I. The system setup is shown in Fig. 12, which consists of a PMSM under test mechanically attached to an induction machine that can have its torque controlled, serving as a mechanical load. A DC supply is adopted to provide constant DC-link voltage, which is set as 200V, and the carrier frequency is 10kHz. A dSPACE

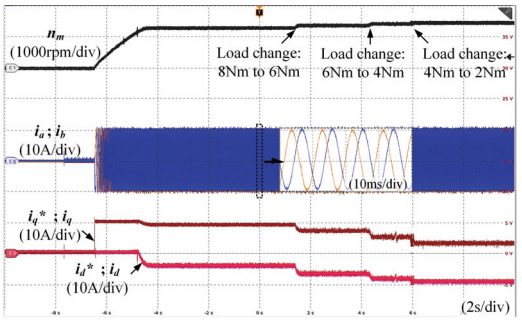

Fig. 13. CVCP system start-up.

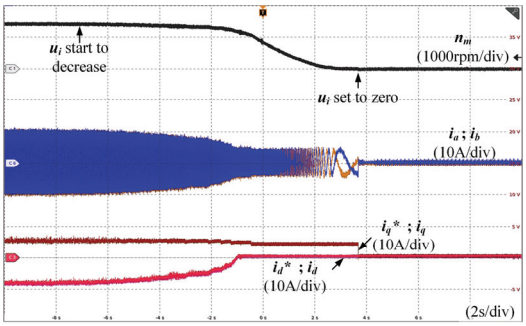

Fig. 14. CVCP system stop.

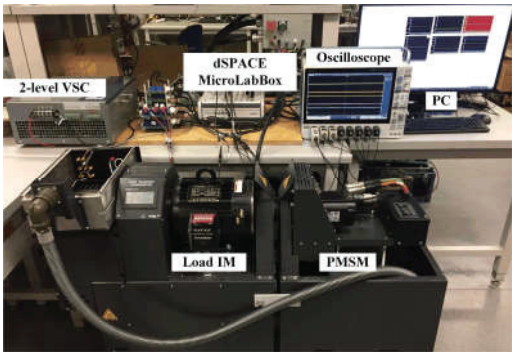

Fig. 12. Experimental setup.

MicroLabBox DS1202 is adopted to implement the control methods.

With the conventional CVCP method, the machine start-up is seen in Fig. 13. To start the system, u_i is commanded from 0 to 1, therefore the motor can speed up to its base speed with maximum torque, when entering the FW region The load torque generated by the induction machine is decreased from 8Nm to 2Nm, in steps of 2Nm. After reaching steady-state with a load of 4Nm, u_i decreases continuously from 1 to 0.4, when it is set to zero. This can be seen in Fig. 14.

TABLE I SYSTEM PARAMETERS

Parameter	Notation	Value
DC-Link Voltage	V_{DC}	200V
Maximum Stator Current	$i_{s,max}$	10A
Stator Resistance	R_s	540mΩ
d-Axis Inductance	L_d	3.1mH
q-Axis Inductance	L_q	3.1mH
Permanent Magnets Flux Linkage	λ_{pm}	150.6mWb
Pole Pairs	p	5
Switching Frequency	f_{sw}	10kHz
Voltage Safety Margin	s_m	0.1

Similar to the CVCP algorithm, the proposed VCLMT is also implemented. The system start-up and stop can be seen in Fig. 15 and 16, respectively. The process is the same as the one used for the CVCP method, in Fig. 13 and 14.

The fact that the machine has its maximum torque during the start-up (by keeping u_i = 1) allows the torque and power profile to be obtained for both algorithms. If a speed control was used, which commonly sees in machine applications, the machine would reach a steady-state point by reducing its torque for speeds close to the reference, making the torque and power curves not show the maximum values for all speeds. During the system stop tests, the speed decreases abruptly when u_i sets to 0.4. This is caused by the fact that the machine torque is close to the load torque for that user input. This behavior is due to the dynamometer operation of the induction machine.

To make a clear comparison, the torque and power comparisons between the two algorithms are shown in Fig. 17 and Fig. 18, respectively. The experimental

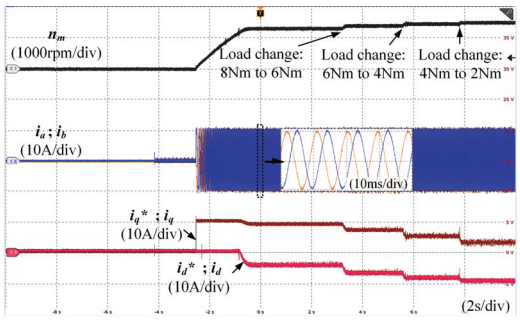

Fig. 15. VCLMT system start-up.

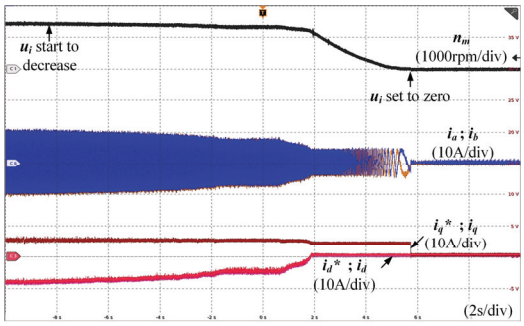

Fig. 16. VCLMT system stop.

comparisons verify that the proposed method allows a higher speed for the same load in the field weakening region; thus, higher power, compared with the conventional CVCP method.

V. Conclusions

Even though the conventional CVCP algorithm produces good results while being simple to implement; however, it fails to utilize the maximum stator voltage which limits its speed operation range. The VCLMT algorithm proposed in this paper optimizes the stator voltage/current trajectory selection to provide better torque and power profiles in the field-weakening region than the conventional algorithm. The proposed method can be implemented without requiring complex optimizations. Moreover, the proposed method can also operate with a variable input, despite not having a linear relationship with the torque in the field weakening mode, which is very suitable for traction applications. The simulation and experimental results verified that the proposed method could reach a wider speed range compared with the conventional method under the field-weakening region.

References

[1] G. Wang, M. Valla and J. Solsona, "Position Sensorless Permanent Magnet Synchronous Machine Drives—A Review," *IEEE Trans. Ind. Electron.*, vol. 67, no. 7, pp. 5830-5842, July 2020.

[2] L. Ding, Y. W. Li and N. R. Zargari, "Discrete-Time SMO Sensorless Control of Current Source Converter-Fed PMSM Drives With Low Switching Frequency," *IEEE Trans. Ind. Electron.*, vol. 68, no. 3, pp. 2120-2129, March 2021

[3] K. T. Chau, C. C. Chan and C. Liu, "Overview of Permanent-Magnet Brushless Drives for Electric and Hybrid Electric Vehicles", *IEEE Trans. Ind. Electron*., vol. 55, no. 6, pp. 2246-2257, 2008.

[4] J. F. Gieras, R-J Wang and M. J. Kamper, *Axial Flux Permanent Magnet Brushless Machines*, Springer, 2008.

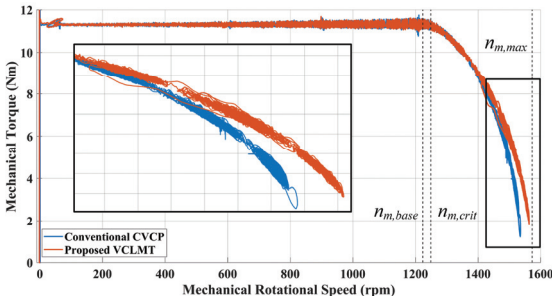

Fig. 17. Experimental torque comparison between algorithms, with the zoom at the high-speed range.

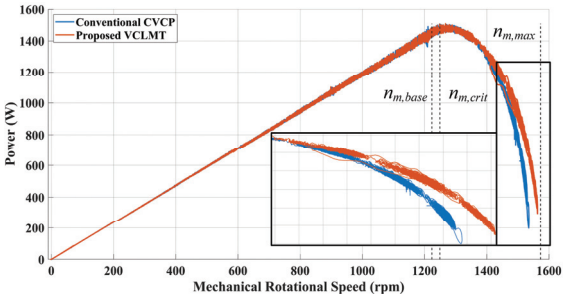

Fig. 18. Experimental power comparison between algorithms, with the zoom at the high-speed range.

[5] D. Moreels and P. Leijnen, "Ths Inside-Out Motor for EVs Is Power Dense and (Finally) Practical", *IEEE Spectrum*, October 2019.

[6] Dongyun Lu and N. C. Kar, "A review of flux-weakening control in permanent magnet synchronous machines," *2010 IEEE Vehicle Power and Propulsion Conference*, Lille, France, 2010.

[7] T. -. Kwon and S. -. Sul, "Novel Antiwindup of a Current Regulator of a Surface-Mounted Permanent-Magnet Motor for Flux-Weakening Control," *IEEE Trans. Ind. Appl.*, vol. 42, no. 5, pp. 1293-1300, Sept.-Oct. 2006.

[8] Q. Hao, D. Mascarella and G. Joos, "Flux-weakening loop design for EV drive with permanent magnet synchronous motor," *2014 IEEE Transportation Electrification Conference and Expo (ITEC)*, Dearborn, MI, USA, 2014.

[9] R. Bojoi, G. Pellegrino, A. Cavagnino and P. Guglielmi, "Direct Flux Vector Control of Axial Flux IPM Motors for in-wheel traction solutions," IECON 2010 - *36th Annual Conference on IEEE Industrial Electronics Society*, Glendale, AZ, USA, 2010.

[10] T. Deng, Z. Su, J. Li, P. Tang, X. Chen and P. Liu, "Advanced Angle Field Weakening Control Strategy of Permanent Magnet Synchronous Motor," *IEEE Trans. on Veh. Technol.*, vol. 68, no. 4, pp. 3424-3435, April 2019.

[11] L. Sepulchre, M. Fadel, M. Pietrzak-David and G. Porte, "MTPV Flux-Weakening Strategy for PMSM High Speed Drive," *IEEE Trans. Ind. Appl.*, vol. 54, no. 6, pp. 6081-6089, Nov.-Dec. 2018.

[12] K. Kim, "A Novel Magnetic Flux Weakening Method of Permanent Magnet Synchronous Motor for Electric Vehicles," *IEEE Trans. on Mag.*, vol. 48, no. 11, pp. 4042-4045, Nov. 2012.

[13] M. Li, "Flux-Weakening Control for Permanent-Magnet Synchronous Motors Based on Z-Source Inverters" M.S. thesis, Marquette University, 2014.

[14] T. Martin and R. Burke, "Practical field weakening current vector control calculations for PMSM in vehicle applications," *2013 World Electric Vehicle Symposium and Exhibition* (EVS27), Barcelona, Spain, 2013.